

Temporal Stability of Metal-Chloride-Doped Chemical-Vapour-Deposited Graphene

Moon H. Kang,^{*,[a]} William I. Milne,^[a, b] and Matthew T. Cole^{*,[a]}

Graphene has proven to be a promising material for transparent flexible electronics.^[1] In this study, we report the development of a transfer and doping scheme of large-area chemical vapour deposited (CVD) graphene. A technique to transfer the as-grown material onto mechanically flexible and optically transparent polymeric substrates using an ultraviolet adhesive (UVA) is outlined, along with the temporal stability of the sheet resistance and optical transparency following chemical doping with various metal chlorides (M_xCl_y). The sheet resistance (R_s) and 550 nm optical transparency ($\%T_{550}$) of the transferred un-doped graphene was $3.5 \text{ k}\Omega \text{ sq}^{-1}$ ($\pm 0.2 \text{ k}\Omega \text{ sq}^{-1}$) and 84.1% ($\pm 2.9\%$), respectively. Doping with AuCl_3 showed a notable reduction in R_s by some 71.4% (to $0.93 \text{ k}\Omega \text{ sq}^{-1}$) with a corresponding $\%T_{550}$ of 77.0%. After 200 h exposure to air at stan-

dard temperature and pressure, the increase in R_s was found to be negligible ($\Delta R_s \text{ AuCl}_3 = 0.06 \text{ k}\Omega \text{ sq}^{-1}$), indicating that, of the considered M_xCl_y species, AuCl_3 doping offered the highest degree of time stability under ambient conditions. There appears a tendency of increasing R_s with time for the remaining metal chlorides studied. We attribute the observed temporal shift to desorption of molecular dopants. We find that desorption was most significant in RhCl_3 -doped samples whereas, in contrast, after 200 h in ambient conditions, AuCl_3 -doped graphene showed only marginal desorption. The results of this study demonstrate that chemical doping of UVA-transferred graphene is a promising means for enhancing large-area CVD graphene in order to realise a viable platform for next-generation optically transparent and mechanically flexible electronics.

1. Introduction

Indium- and fluorine-doped tin oxide (ITO/FTO) have gained significant traction as transparent electrodes in large-area electronics. Though concurrently offering high optical transparency and high electrical conductivity, such oxides are, however; particularly brittle.^[2] Graphene, an atomically thin layer of hexagonally latticed carbon atoms, has been widely proposed as an alternative. Its high charge mobility, high optical transmittance, alongside its impressive mechanical robustness and flexibility make it well-suited for a number of emerging optoelectronic applications, such as e-paper, flexible displays and user-conformal wearable devices.^[3] To date, there have been many attempts to utilise graphene as a transparent flexible conductor in organic light-emitting diodes (OLED),^[3b,4] touch screens^[5] and photovoltaic cells.^[6] Common to all such optoelectronic applications is the need for a reduction in the sheet resistance (R_s) of graphene whilst maintaining its high optical transparency. Unlike metals, graphene has a conical band structure.^[3] Owing to the low density of states at the Fermi level in pristine graphene, the R_s of monolayer graphene is fundamentally lim-

ited to a few $\text{k}\Omega \text{ sq}^{-1}$. This is deemed too high for most commercial applications; touch screens require $R_s < 500 \Omega \text{ sq}^{-1}$, whereas graphical displays require $R_s < 100 \Omega \text{ sq}^{-1}$ alongside flat-band transparencies in excess of 90% across the optical spectrum.^[7] One approach to reduce R_s is to shift the Fermi level through selective doping.

Chemical doping has been considered one of the most viable means of decreasing the R_s without dramatically compromising the optical transparency.^[8] In the present study, we adopted a chemical doping methodology based on established chlorine compounds that have been investigated elsewhere in other nanocarbon systems.^[8c, f, 9] The spatial and temporal variation in R_s and the optical transparency ($\%T$) are investigated. Doped samples showed an appreciable change in performance (AuCl_3 : 9% decrease in R_s), even after exposure to air for 200 h, highlighting the potential of doped, unencapsulated, two-dimensional optoelectronic devices.

2. Results and Discussion

Graphene was grown using chemical vapour deposition (CVD). As-synthesised graphene was then transferred onto polyethylene terephthalate (PET) substrates through an inherently scalable ultraviolet adhesive (UVA)-transfer method, as reported elsewhere.^[10] Following UVA transfer, the graphene was chemically doped with one of five chloride compounds (AuCl_3 , FeCl_3 , SnCl_2 , IrCl_3 or RhCl_3) to systematically study their effects on the graphene supports conductivity. For such chemical doping, each compound was dissolved in different solvents [AuCl_3 and

[a] M. H. Kang, Prof. W. I. Milne, Dr. M. T. Cole
Electrical Engineering Division, Department of Engineering
University of Cambridge
CB3 0FA, Cambridge (United Kingdom)
E-mail: mhk29@cam.ac.uk
mtc35@cam.ac.uk

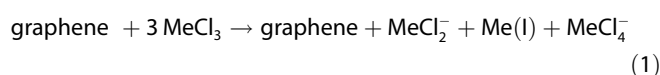
[b] Prof. W. I. Milne
College of Information Science and Electronic Engineering,
Zhejiang University,
310027, Hangzhou (P. R. China)

IrCl₃/acetonitrile, FeCl₃ and SnCl₂/deionised (DI) water, and RhCl₃/methanol], each at 20 mM concentration. The dopant solutions were spin-cast onto the transferred graphene samples at 2000 rpm for 1 min.

To assess the implications of the M_xCl_y doping, it is necessary to decouple any shifts in R_s and %T associated with the solvent from those of the M_xCl_y solute. Figure 1 summarises the solvent and concentration controls. In the solvent controls, three high-purity solvents (DI water, methanol and acetonitrile) were spin-coated onto the graphene using the same casting recipe as those used for the M_xCl_y doping, and %T and R_s were subsequently measured. As shown in Figures 1a and 1b, there was no significant change in %T (Δ%T = +0.75, +0.7 and +0.11% for samples treated with DI water, methanol and acetonitrile, respectively). Similarly, there was no significant change in R_s (ΔR_s = +0.013 and -0.027 kΩ sq⁻¹ for samples treated with DI water and methanol, respectively); however, samples treated with acetonitrile showed a non-negligible increase in R_s (+0.245 kΩ sq⁻¹). Acetonitrile degraded R_s. In the present study, AuCl₃ was dissolved in acetonitrile. Interestingly, our AuCl₃ samples showed the largest decrease in R_s, even though the doping effects of acetonitrile evidently tend to increase R_s. One clear strategy to further improve the doping effects of AuCl₃ would be to use an alternative solvent. Nevertheless, Fig-

ures 1a and 1b reveal that the impact of the solvent is largely negligible, relative to the M_xCl_y solute, suggesting that the observed variations in R_s and %T, upon M_xCl_y doping, are not attributed to the solvent, but rather the solute. Figures 1c and 1d show %T and R_s values of the doped graphene as a function of concentration (AuCl₃). As the dopant concentration increased a lower %T and lower R_s was evident. %T was substantially decreased (Δ%T = 10.39%) at 40 mM, even though the R_s did not notably decrease; R_s exhibited a comparable value for the reduction at 30 mM (ΔR_s = 1.941 kΩ sq⁻¹) and 20 mM (ΔR_s = 2.184 kΩ sq⁻¹). The normalised Δ%T and ΔR_s of the doped graphene on PET with the five kinds of dopant solution, as shown in Figures 1e and 1f, suggest that R_s is not directly proportional to the dopant concentration, whilst the %T decreases consistently with increasing the concentration. These results indicate that the dopant molecules may adsorb onto the graphene surface, resulting in a %T decrease, but the charge transfer from the dopant molecules evidently saturates at concentrations in excess of 20 mM. The reduction of R_s appears to relate to the degree of electronegativity of the metal ions.^[11] As shown in Figure 1f, the largest reduction in R_s (ΔR_s/R₀ = 0.841) was observed for doping with AuCl₃-doped graphene, which has the highest electronegativity (2.54) of the dopants considered (FeCl₃: 1.83, SnCl₂: 1.96, IrCl₃: 2.2 and RhCl₃: 2.28). Similar trends in R_s and metal-constituent electronegativity were noted throughout. Additional transport studies will be reported elsewhere.

Chemical doping was adopted as it does not induce significant mechanical modification of the graphene backbone, unlike substitutional doping, which is typically achieved through aggressive plasma-based processing. The metal-chloride molecules in solution mediate effective charge transfer to the graphene basal plane. The molecules are physically adsorbed, mediating spontaneous charge transfer across well-defined energy levels at the graphene-metal-ion interface. In the present system, the expected reaction between the metal chloride and graphene is given by Equations (1)–(3):^[9a]



The positive Me³⁺ ions in MeCl₄⁻ are neutralised following charge donation to the graphene substrate. Depending on the metal type, the positive reduction potentials of the metal ions result in the removal of a given proportion of the local electron population from the graphene substrate, thereby mediating p-type doping. The dispersed SnCl₂ interaction differs from that of the other four considered metal chlorides. SnCl₂ reacts in H₂O, producing Sn(OH)Cl and HCl,^[12] according to Equation (4):

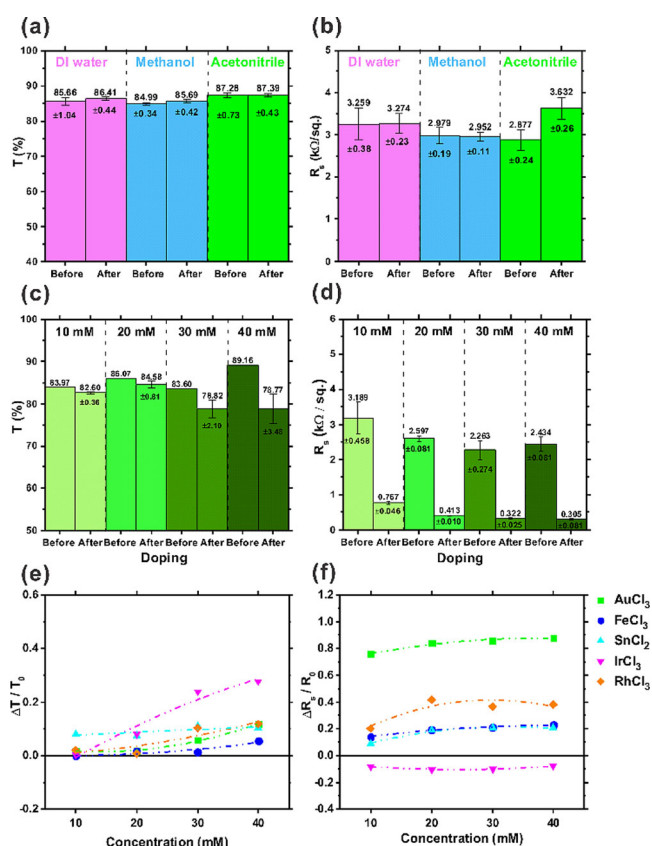
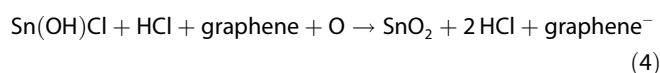


Figure 1. Solvent controls: a) %T (550 nm) and b) R_s of graphene on PET following solvent treatment (without dopant). c) %T (550 nm) and d) R_s of AuCl₃-doped graphene for various molar concentrations. e) Normalised %T change and f) R_s change of doped graphene for all M_xCl_y as a function of molar concentrations.

Aqueous SnCl_2 behaves as a reducing agent. Sn^{2+} reacts with bound oxygen species, deposited during ambient exposure. When the oxygen constituent is removed, the graphene becomes increasingly negatively charged, leading to n-type doping. The standard reduction potential of Sn^{2+} is negative (-0.19 V),^[13] it has a tendency to donate electrons to the graphene substrate, whereas the remaining four dopants have positive standard potentials (AuCl_3 : 1.002 V , FeCl_3 : 0.77 V , IrCl_3 : 1.156 V and RhCl_3 : 0.76 V).^[13] Thus, graphene doped with AuCl_3 , FeCl_3 , IrCl_3 and RhCl_3 will likely show nominally p-type behaviour, whereas SnCl_2 -doped graphene would exhibit nominally n-type behaviour. Indeed, our Raman spectroscopy findings [2D peak shift: 14.64 cm^{-1} (AuCl_3), 2.86 cm^{-1} (FeCl_3), -2.04 cm^{-1} (SnCl_2), -4.54 cm^{-1} (IrCl_3) and 1.30 cm^{-1} (RhCl_3)] largely confirm this hypothesis. The anomalous Raman behaviour of IrCl_3 is under further investigation. Although the charge polarity of the doped graphene varies, it remains true that all of the various metal chlorides studied induce an increase in the charge carrier population, thereby increasing the carrier density and, hence, lowering R_S . Additionally, consistent with reports elsewhere, we find that the dopant molecules are prone to adhere to defects, vacancies, grain boundaries and other high-surface-potential non-idealities within the graphene basal plane. Chang et al. showed that adatoms on graphene have a tendency to dwell on atomic steps or boundaries.^[14] Without degrading the lattice periodicity, the readily adsorbed dopant molecules easily bind to boundaries and cracks and heal them, providing additional charge-transport routes, especially throughout particularly defective micro-sized areas.

Figures 2a and 2b are photographs of $20\text{ mm} \times 20\text{ mm}$ as-grown graphene on Cu foil and a UVA-transferred sample, respectively. Figures 2c and 2d show the spatial variation in % T at 550 nm (% T_{550}) (ATI, Unicam UV2). Figures 2e and 2f depict the R_S variation of un-doped and AuCl_3 -doped graphene, respectively. Full spectra were acquired at each measured position. Figure 2g summarises the mean % T maps for all of the dopants considered. The % T_{550} of the un-doped graphene was 84.1% , some 5.2% lower than that in bare PET (89.3%), suggesting that the graphene is principally mono- and bilayer. Corroborating polychromatic Raman analysis, suggests a largely monolayer material with a D-to-G band intensity ratio (I_D/I_G) of approximately 2.05 and a I_{2D}/I_G ratio of 0.29 . The remaining optical absorption is attributed to the $5\text{ }\mu\text{m}$ -thick UVA. The standard deviation in the spatially resolved % T of the un-doped graphene on PET suggests that the UVA-transfer method led to an areal uniformity of approximately 2.9% , with an optical absorption ranging from 2.3 to 8.1% across the sample ($20\text{ mm} \times 20\text{ mm}$). After chemical doping, the areal mean % T_{550} decreased by 7.0 (RhCl_3), 19.2 (IrCl_3), 7.1 (AuCl_3), 7.5 (FeCl_3) and 10.3% (SnCl_2).

Figures 2e and 2f show the spatially resolved R_S (Jandel four-point probe) of the un-doped and doped graphene on PET. The UVA-transferred graphene showed an R_S value of $3.5 \pm 0.2\text{ k}\Omega\text{sq}^{-1}$. By way of a control, to compare the R_S of the UVA-transferred graphene to that of conventional poly(methyl methacrylate) (PMMA)-transferred graphene, we assessed the conductivity of as-grown graphene, independently, by transfer-

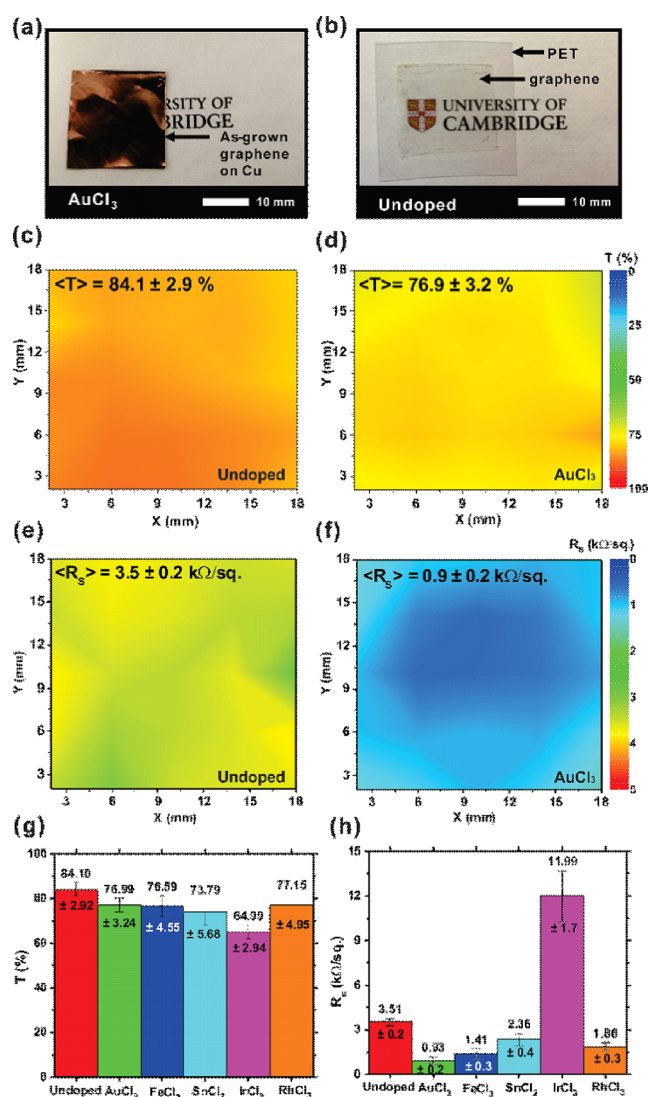


Figure 2. Photographs of typical a) as-grown graphene on Cu foil and b) transferred graphene onto PET. % T maps (550 nm) of c) un-doped graphene and d) AuCl_3 -doped graphene. R_S maps of e) un-doped graphene and f) AuCl_3 -doped graphene, and bar charts of mean values of g) % T and h) R_S of un-doped graphene and graphene doped with five different metal chlorides.

ring it to quartz substrates. The PMMA-transferred graphene showed an R_S of $5.5 \pm 1.2\text{ k}\Omega\text{sq}^{-1}$, which is some 64% higher than that of UVA-transferred graphene. Clearly, the transfer method plays a critical role in optimising R_S . As shown in Figure 2h, AuCl_3 doping afforded the lowest R_S ($0.9 \pm 0.2\text{ k}\Omega\text{sq}^{-1}$), showing a rather dramatic decrease ($\Delta R_S = 2.6\text{ k}\Omega\text{sq}^{-1}$). The highest R_S was observed for the IrCl_3 -doped graphene ($12.0 \pm 1.7\text{ k}\Omega\text{sq}^{-1}$). Graphene electrodes are attractive for the flexible display industry; however, spatial uniformity in R_S is key if such materials are to be adopted widely in emerging flexible display panels. The R_S and its spatial uniformity intimately dictate light emission uniformity. Following UVA transfer, the R_S spatial distribution (measured over 4 cm^2) for the un-doped graphene was found to be very uniform ($\pm 0.2\text{ k}\Omega\text{sq}^{-1}$), which was maintained even after chemical doping with AuCl_3 ($\pm 0.2\text{ k}\Omega\text{sq}^{-1}$),

FeCl_3 ($\pm 0.3 \text{ k}\Omega \text{sq}^{-1}$), SnCl_2 ($\pm 0.4 \text{ k}\Omega \text{sq}^{-1}$) and RhCl_3 ($\pm 0.3 \text{ k}\Omega \text{sq}^{-1}$). The transfer, rather than the growth or doping procedure, broadly dominates the spatial uniformity in R_s . However, the distribution of the R_s standard deviation in IrCl_3 -doped graphene ($\pm 1.7 \text{ k}\Omega \text{sq}^{-1}$) was significantly higher than in the un-doped case ($\pm 0.2 \text{ k}\Omega \text{sq}^{-1}$), suggesting that, in such systems, the doping procedure dominates the final uniformity. Inspection by scanning electron microscopy (SEM) suggests that the agglomeration of large Ir precipitates ($14.4 \pm 3.7 \mu\text{m}$ in diameter) is the likely cause for this reduced spatial uniformity, with the other Me_xCl_y precipitates being about ten times smaller on average. AuCl_3 is the most effective dopant, showing a markedly lower R_s value ($0.9 \pm 0.2 \text{ k}\Omega \text{sq}^{-1}$), with a decrease in % T of only 7.1% (Figures 2g and 2h).

To assess the time evolution of the doping, % T_{550} and R_s were measured immediately after doping and at fixed time points thereafter, as illustrated in Figures 3a and 3b. An ideal transparent conductor necessitates time-invariant % T_{550} and R_s . However, as previously reported,^[8b,9b] although dopants reduce the R_s value, they also often reduce % T , with deleterious temporal variations in both. For all of our samples, the transmittance decreased following doping, as shown in Figure 3a. After exposure to air for 200 h, un-doped graphene maintained its initial % T and R_s with only a small reduction ($\Delta\%T = -0.8\%$ and $\Delta R_s = -4.53 \text{ }\Omega \text{sq}^{-1}$). For the transmittance of the doped samples, a recovery process was observed, with the transmittance tending to increase, though only marginally so, with time. The most substantial increase was observed for AuCl_3 -doped graphene ($\Delta\%T = 1.9\%$). This increase is presumed to be associated with time-dependent desorption of physisorbed dopants, activated by ambient thermal excitation.^[9c,16] Desorption also underpins the variation in R_s ; however, to a somewhat much lesser extent. The increase in R_s , for AuCl_3 -doped graphene, was largely negligible ($0.85 \rightarrow 0.93 \text{ }\Omega \text{sq}^{-1}$). The largest

time-dependent change in R_s was observed for FeCl_3 -doped graphene ($1.81 \rightarrow 2.26 \text{ }\Omega \text{sq}^{-1}$). All doped samples showed an increase in R_s , though often by comparatively small shifts.

The ratio of the optical conductance (σ_{opt}) to the dc electronic conductance (σ_{dc}) defines a figure of merit of the optoelectronic performance of transparent conductors [Eq. (5)]:^[15a,17]

$$T = \left[1 + \left(\frac{tZ_0}{2} \sigma_{\text{opt}} \right)^2 \right]^{-2} = \left[1 + 188.5 \frac{1}{R_s} \left(\frac{\sigma_{\text{opt}}}{\sigma_{\text{dc}}} \right) \right]^{-2} \quad (5)$$

Here, Z_0 is the impedance of free space ($377 \text{ }\Omega$) and t is the film thickness. For an ideal transparent conductive electrode, $\sigma_{\text{opt}}/\sigma_{\text{dc}} \rightarrow 0$; this necessitates a low sheet resistance and concurrently high optical transmittance. The approximate $\sigma_{\text{opt}}/\sigma_{\text{dc}}$ values of our doped transferred graphene, alongside competing transparent flexible conductors, are plotted in Figures 3c and 3d. A low $\sigma_{\text{opt}}/\sigma_{\text{dc}}$ value denotes a material with a low sheet resistance and high optical transmittance. For all doped samples, excluding IrCl_3 , $\sigma_{\text{opt}}/\sigma_{\text{dc}} < 1.40$. $\langle \sigma_{\text{opt}}/\sigma_{\text{dc}} \rangle = 0.74$ for the AuCl_3 -doped sample during the entire measurement period. Though still some way off the industry ITO/FTO standard (0.029), these un-optimised devices show promise. Our surface metrology suggests that dopant agglomeration at defects and grain edges is critical in healing the otherwise imperfect, non-contiguous transferred graphene, with AuCl_3 doping being the most efficient of the M_xCl_y considered.

During casting, dopant molecules are physically adsorbed onto the graphene. Owing to the inhomogeneous nature of molecular binding, we believe that the surface energy of graphene increases following chemical doping. The contact angles (θ) of un-doped and doped graphene samples were measured using water and ethylene glycol probes (CA M200, LOT-Oriel Ltd.). The time-dependent contact angle with water is shown in Figure 4b. After doping, the contact angle initially decreased from 76.4° (un-doped) to 63.1° (AuCl_3), 62.6° (FeCl_3), 69.5° (SnCl_2), 23.2° (IrCl_3) and 62.5° (RhCl_3). After exposure to air for 200 h, the contact angle increased in FeCl_3 (76.7°), RhCl_3 (74.3°) and IrCl_3 (54.2°), whereas there was no substantial change in the AuCl_3 (62.5°) or SnCl_2 (70.3°) cases. The surface energy can be calculated by substituting the Young's equation ($\gamma_s = \gamma_{\text{LV}} \cos \theta + \gamma_{\text{SL}}$) into the Owens–Wendt model^[18] to give Equation (6):

$$\gamma_{\text{LV}}(\cos \theta + 1) = 2(\gamma_s^d \gamma_{\text{LV}}^d)^{1/2} + 2(\gamma_s^p \gamma_{\text{LV}}^p)^{1/2} \quad (6)$$

Here, γ_{SL} is the surface energy of the interface of the solid surface and liquid, γ_{LV} is the surface energy of the liquid, γ_s is the surface energy of the solid ($= \gamma_s^d + \gamma_s^p$, where γ_s^d is the dispersion term of the surface energy of the solid and γ_s^p is the polar term of surface energy of the solid). At room temperature and ambient pressure, the surface energy of water is 72.8 mN m^{-1} ($= \gamma_{\text{LV}}^d + \gamma_{\text{LV}}^p = 24.7 + 48.1$, where γ_{LV}^d is the dispersion term of surface energy of the liquid and γ_{LV}^p is the polar term of the liquids surface energy) and that of ethylene glycol is 48.3 mN m^{-1} ($= \gamma_{\text{LV}}^d + \gamma_{\text{LV}}^p = 30.9 + 17.4$).^[19]

As plotted in Figure 5a, the surface energy of un-doped graphene is 29.4 mJ m^{-2} . After doping, it increases to 38.8 mJ m^{-2}

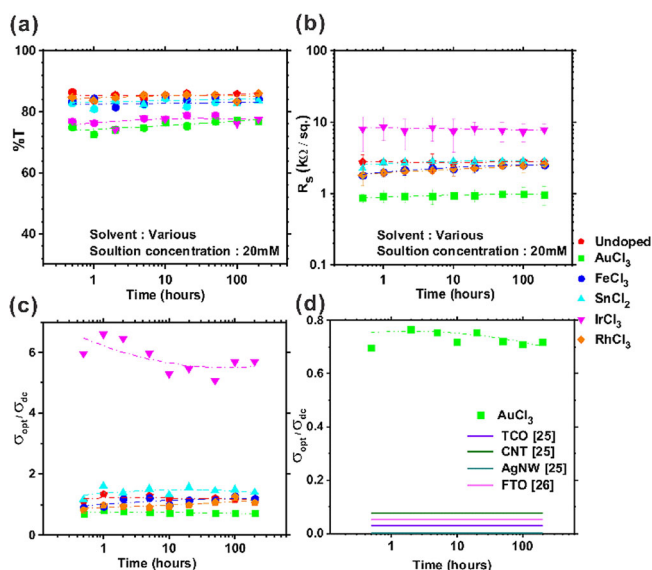


Figure 3. Time-dependent properties of chemically doped graphene on PET under ambient conditions: a) % T , b) R_s of doped graphene, c) ratio of optical conductivity to dc electrical conductivity and d) comparison of the ratio to other conductive transparent media.^[15]

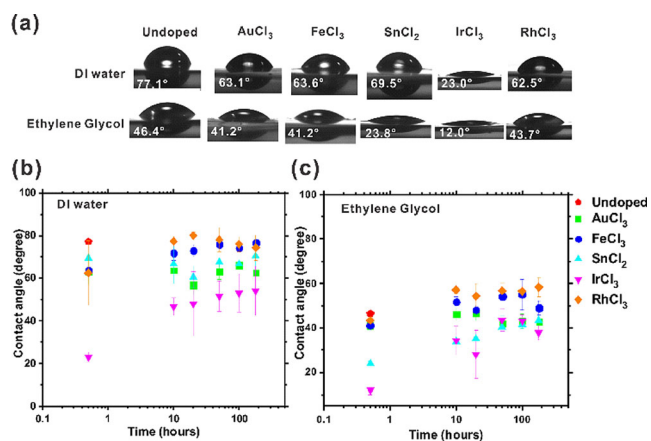


Figure 4. a) Photographs of water and ethylene glycol droplets on chemically doped graphene for measuring the contact angles. Time-dependent contact angles measured by using b) DI water and c) ethylene glycol.

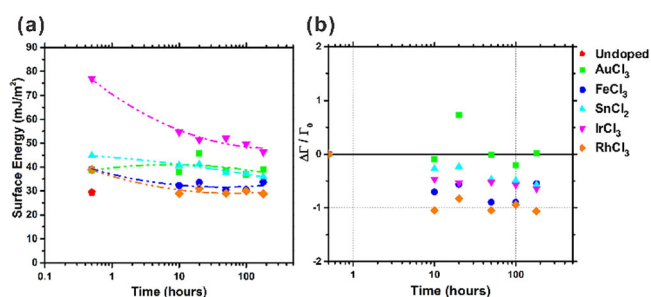


Figure 5. Time-dependent variation of a) the surface energy and b) the surface concentration of chemically doped graphene with metal chlorides.

(AuCl₃), 39.0 mJ m⁻² (FeCl₃), 44.7 mJ m⁻² (SnCl₂), 76.9 mJ m⁻² (IrCl₃) and 38.9 mJ m⁻² (RhCl₃). After 200 h, the surface energy decreases for FeCl₃ (33.7 mJ m⁻²), SnCl₃ (36.0 mJ m⁻²), IrCl₃ (46.3 mJ m⁻²) and RhCl₃ (28.8 mJ m⁻²). This change in surface energy is consistent with our earlier %*T* and *R*_s findings. Upon metal-chloride doping of graphene, there is a measurable increase in surface energy, owing to the deposition of local agglomerates and precipitates, empirically verified by our surface energy measurements and corroborated, by proxy, in the measured decreases in %*T* and *R*_s. After 200 h, some of the adsorbed FeCl₃, SnCl₂, IrCl₃ and RhCl₃ molecular agglomerates are desorbed upon air exposure, with samples subsequently exhibiting a decrease in surface energy and increase in *R*_s. Conversely, AuCl₃ showed a slight increase in surface energy, even after 200 h of air exposure at standard temperature and pressure ($\Delta\gamma = 0.18$ mJ m⁻²). This increase seems to arise from, not only the much smaller amount of the dopant molecule desorption than other four doped samples, but also possible atmospheric oxygen adsorption. Attachment of oxygen tends to also increase the surface energy. To evaluate the extent of molecular desorption, the change in surface concentration was calculated from the Gibb's isotherm, as given in Equation (7):^[20]

$$d\gamma = - \sum_i \Gamma_i d\mu_i \quad (7)$$

where, γ is the surface energy, $d\mu_i$ is the change in chemical potential, and Γ_i is the concentration of adsorbed molecules on the surface, which is termed the surface excess. At constant temperature, Γ is given by Equation (8):^[20]

$$\Gamma = - \frac{1}{RT} \left(\frac{d\gamma}{d\ln C} \right)_T \quad (8)$$

Using Equation (8), the temporal variation of the surface concentration ($\Delta\Gamma$) in the doped graphene was calculated, and is shown in Figure 5b. Γ_0 is the surface concentration at $t = 0$ s, immediately upon doping, and C is the concentration of dopant in solution.

Figure 5b highlights the marked migration of dopant molecules away from, and attached to, the graphene surface. A negative $\Delta\Gamma/\Gamma_0$, with decreasing Γ indicates that the molecules are desorbed from the surface, whereas positive $\Delta\Gamma/\Gamma_0$ suggests the adsorption of molecules. The desorption case is trivial, with the net migration of local adsorbates, deposited during the doping process, moving away from the surface. For AuCl₃-doped graphene, $\Delta\Gamma/\Gamma_0 = 0.019$ (after 200 h). The positive $\Delta\Gamma/\Gamma_0$ value implies that impurities, likely ambient oxygen, are adsorbed onto the graphene surface, with absorption rates well within the timeframe of study. The adsorption of ambient oxygen on nanocarbons is well established.^[21] The negative values of $\Delta\Gamma/\Gamma_0$ for FeCl₃-doped (-0.549), SnCl₃-doped (-0.572), IrCl₃-doped (-0.644) and RhCl₃-doped graphene (-1.064) indicate increasing desorption. These results are consistent with the temporal variation in *R*_s; the time-varying increase in *R*_s was lowest for AuCl₃-doped graphene (0.08 k Ω sq⁻¹). Therefore, it is apparent that the resistance increase with time can be principally attributed to the time-dependent desorption of dopant molecules, highlighting the merits of polymer passivation and hermetic capping layers to prevent degradation of graphene-based electronics under ambient conditions.

3. Conclusions

Metal-chloride-doped graphene has much promise as a transparent conductor for flexible electronics. AuCl₃-doped graphene exhibits a conductance ratio $\sigma_{\text{opt}}/\sigma_{\text{dc}}$ of 0.70, which increased by only 0.01 after 200 h under ambient conditions. Molecular desorption was repeatedly implicated as the chief driver underpinning temporal variations in sheet resistance of metal-chloride doped graphene, with the lowest normalised change in surface energy ($\Delta\Gamma/\Gamma_0$) being from FeCl₃-doped graphene (-0.942), which demonstrated the largest desorption rate which resulted in the largest time-dependent increase in *R*_s (0.45 k Ω sq⁻¹). Our experimental results herein indicate that metal-chloride doping of graphene is a useful step in realising flexible transparent electronics, especially when used in conjunction with hermetically sealing encapsulation layers.

Acknowledgements

M.T.C. thanks the Oppenheimer Research Trust for generous financial support.

Keywords: adsorption · chemical doping · graphene · surface energy · transparent flexible conductors

- [1] a) S. K. Lee, K. Rana, J. H. Ahn, *J. Phys. Chem. Lett.* **2013**, *4*, 831–841; b) X. Huang, T. Leng, M. Zhu, X. Zhang, J. Chen, K. Chang, M. Aqeeli, A. K. Geim, K. S. Novoselov, Z. Hu, *Sci. Rep.* **2015**, *5*, 18298.
- [2] a) T. M. G. Paradee, A. Christou, *IEEE Tran. Dev. Mater. Rel.* **2015**, *15*, 423–428; b) Q. Zhang, Y. Di, C. M. Huard, L. J. Guo, J. Wei, J. Guo, *J. Mater. Chem. C* **2015**, *3*, 1528–1536.
- [3] a) K. S. Novoselov, A. K. Geim, S. V. Morozov, D. Jiang, Y. Zhang, S. V. Dubonos, I. V. Grigorieva, A. A. Firsov, *Science* **2004**, *306*, 666–669; b) S. Bae, H. Kim, Y. Lee, X. F. Xu, J.-S. Park, Y. Zheng, J. Balakrishnan, T. Lei, H. Ri Kim, Y. I. Song, Y.-J. Kim, K. S. Kim, B. Ozyilmaz, J.-H. Ahn, B. H. Hong, S. Iijima, *Nat. Nanotechnol.* **2010**, *5*, 574–578; c) A. K. Geim, *Science* **2009**, *324*, 1530–1534; d) X. Li, Y. Zhu, W. Cai, M. Borysiak, B. Han, D. Chen, R. D. Piner, L. Colombo, R. S. Ruoff, *Nano Lett.* **2009**, *9*, 4359–4363.
- [4] a) T.-H. Han, Y. Lee, M.-R. Choi, S.-H. Woo, S.-H. Bae, *Nat. Photonics* **2012**, *6*, 105–110; b) S.-Y. Kim, J.-J. Kim, *Org. Electron.* **2012**, *13*, 1081–1085; c) J. Wu, M. Agrawal, H. A. Becerril, Z. Bao, Z. Liu, *ACS Nano* **2010**, *4*, 43–48.
- [5] a) J. Lee, M. T. Cole, J. C. S. Lai, A. Nathan, *J. Disp. Technol.* **2014**, *10*, 362–366; b) K. Jaeho, I. Masatou, K. Yoshinori, T. Kazuo, H. Masataka, I. Sumio, *Appl. Phys. Lett.* **2011**, *98*, 091502.
- [6] a) P. Lin, W. C. H. Choy, D. Zhang, F. Xie, J. Xin, C. W. Leung, *Appl. Phys. Lett.* **2013**, *102*, 113303; b) H. Park, P. R. Brown, V. Bulovic, J. Kong, *Nano Lett.* **2012**, *12*, 133–140; c) Y. Un Jung, S.-I. Na, H.-K. Kim, S. Jun Kang, *J. Vac. Sci. Technol. A* **2012**, *30*, 050604.
- [7] S. Ray, *Applications of Graphene and Graphene-Oxide based Nanomaterials*, Elsevier Science **2015**.
- [8] a) U. Dettlaff-Weglikowska, V. Skakalova, R. Graupner, S. H. Jhang, B. H. Kim, H. J. Lee, L. Ley, Y. W. Park, S. Berber, D. Tomanek, S. Roth, *J. Am. Chem. Soc.* **2005**, *127*, 5125–5131; b) F. Güneş, H. J. Shin, C. Biswas, G. H. Han, E. S. Kim, S. J. Chae, J. Y. Choi, Y. H. Lee, *ACS Nano* **2010**, *4*, 4595–4600; c) A. Kasry, M. A. Kuroda, G. J. Martyna, G. S. Tulevski, A. A. Bol, *ACS Nano* **2010**, *4*, 3839–3844; d) H. J. Shin, W. M. Choi, D. Choi, G. H. Han, S. M. Yoon, H. K. Park, S. W. Kim, Y. W. Jin, S. Y. Lee, J. M. Kim, J. Y. Choi, Y. H. Lee, *J. Am. Chem. Soc.* **2010**, *132*, 15603–15609; e) X. Li, D. Xie, H. Park, M. Zhu, T. H. Zeng, K. Wang, J. Wei, D. Wu, J. Kong, H. Zhu, *Nanoscale* **2013**, *5*, 1945–1948; f) H.-Z. Geng, K. K. Kim, C. Song, N. T. Xuyen, S. M. Kim, K. A. Park, D. S. Lee, K. H. An, Y. S. Lee, Y. Chang, Y. J. Lee, J. Y. Choi, A. Benayad, Y. H. Lee, *J. Mater. Chem.* **2008**, *18*, 1261–1266; g) D. Hee Shin, J. Min Kim, C. Wook Jang, J. Hwan Kim, S. Kim, S.-H. Choi, *J. Appl. Phys.* **2013**, *113*, 064305.
- [9] a) M. S. A. Abdou, S. Holdcroft, *Chem. Mater.* **1996**, *8*, 26–31; b) R. Ishikawa, M. Bando, Y. Morimoto, A. Sandhu, *Nanoscale Res. Lett.* **2011**, *6*, 111; c) K. C. Kwon, B. J. Kim, J.-L. Lee, S. Y. Kim, *J. Mater. Chem. C* **2013**, *1*, 2463–2469.
- [10] M. H. Kang, W. I. Milne, M. T. Cole, *IET Circuits, Devices & Systems* **2015**, *9*, 39–45; *Systems* **2015**, *9*, 39–45.
- [11] a) K. K. Kim, S. M. Kim, Y. H. Lee, *Acc. Chem. Res.* **2016**, *49*, 390–399; b) *Compendium of chemical terminology*, 2nd ed., IUPAC, **1997**.
- [12] S. Li, Y. Wang, C. Lai, J. Qiu, M. Ling, W. Martens, H. Zhao, S. Zhang, *J. Mater. Chem. A* **2014**, *2*, 10211–10217.
- [13] J. A. Dean, *Lange's handbook of chemistry*, 15th ed., McGraw-Hill Book Company, **1979**.
- [14] H. Chang, M. Saito, T. Nagai, Y. Liang, Y. Kawazoe, Z. Wang, H. Wu, K. Kimoto, Y. Ikuhara, *Sci. Rep.* **2014**, *4*.
- [15] a) S. De, T. M. Higgins, P. E. Lyons, E. M. Doherty, P. N. Nirmalraj, W. J. Blau, J. J. Boland, J. N. Coleman, *ACS Nano* **2009**, *3*, 1767–1774; b) A. E. Rakhshani, Y. Makdisi, H. A. Ramazaniyan, *J. Appl. Phys.* **1998**, *83*, 1049–1057.
- [16] a) S. Tongay, K. Berke, M. Lemaitre, Z. Nasrollahi, D. B. Tanner, A. F. Hebard, B. R. Appleton, *Nanotechnology* **2011**, *22*, 425701; b) H. Liu, Y. Liu, D. Zhu, *J. Mater. Chem.* **2011**, *21*, 3335–3345; c) K. C. Kwon, B. J. Kim, J.-L. Lee, S. Y. Kim, *J. Mater. Chem.* **2013**, *1*, 253–259.
- [17] S. De, P. J. King, M. Lotya, A. O'Neill, E. M. Doherty, Y. Hernandez, G. S. Duesberg, J. N. Coleman, *Small* **2010**, *6*, 458–464.
- [18] D. K. Owens, R. C. Wendt, *J. Appl. Polym. Sci.* **1969**, *13*, 1741.
- [19] I. Moutinho, M. Figueiredo, P. Ferreira, *Tappi J.* **2007**, *6*, 26–32.
- [20] D. K. Chattoraj, *Adsorption and the Gibbs surface excess*, Plenum Publishing Corporation, New York **1984**.
- [21] a) C. Mathieu, B. Lalmi, T. O. Montes, E. Pallecchi, A. Locatelli, S. Latil, R. Belkhou, A. Ouerghi, *Phys. Rev. B* **2012**, *86*; b) F. Nasehnia, M. Seifi, *Modern Physics Letters B* **2014**, *28*.

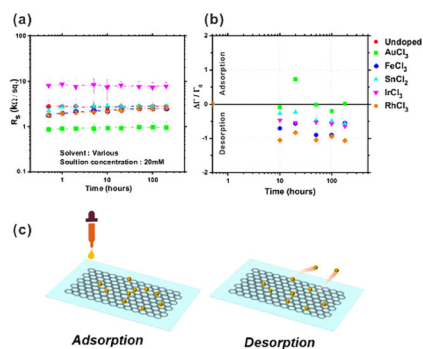
Manuscript received: March 14, 2016

Accepted Article published: May 11, 2016

Final Article published: ■ ■ ■, 2016

ARTICLES

Be flexible! The temporal stability of metal-chloride doping of graphene is investigated. Doping graphene and thereby decreasing its sheet resistance is a key step to make use of it in flexible electronics. The temporal evolution of the electrical resistance as a function of metal chloride exposure are investigated herein.



M. H. Kang, W. I. Milne, M. T. Cole**



Temporal Stability of Metal-Chloride-Doped Chemical-Vapour-Deposited Graphene